Interfacial mechanism studies of electroless plated Cu films on a -Ta:N layers catalyzed by PIII

Jian-Hong Lin, Tzu-Li Lee, Wei-Jen Hsieh, Chien-Cheng Lin, Chwung-Shan Kou, and Han C. Shih

Citation: Journal of Vacuum Science & Technology A **20**, 733 (2002); doi: 10.1116/1.1465448
View online: http://dx.doi.org/10.1116/1.1465448
View Table of Contents: http://scitation.aip.org/content/avs/journal/jvsta/20/3?ver=pdfcov
Published by the AVS: Science & Technology of Materials, Interfaces, and Processing

Interfacial mechanism studies of electroless plated Cu films on *a*-Ta:N layers catalyzed by PIII

Jian-Hong Lin
Department of Materials Science and Engineering, National Tsing Hua University, Hsinchu, Taiwan 300, Republic of China

Tzu-Li Lee
Department of Materials Science and Engineering, National Chiao Tung University, Hsinchu, Taiwan 300, Republic of China

Wei-Jen Hsieh
Department of Materials Science and Engineering, National Tsing Hua University, Hsinchu, Taiwan 300, Republic of China

Chien-Cheng Lin
Department of Materials Science and Engineering, National Chiao Tung University, Hsinchu, Taiwan 300, Republic of China

Chwung-Shan Kou
Department of Physics, National Tsing Hua University, Hsinchu, Taiwan 300, Republic of China

Han C. Shih[a)]
Department of Materials Science and Engineering, National Tsing Hua University, Hsinchu, Taiwan 300, Republic of China

(Received 26 October 2001; accepted 4 February 2002)

This study evaluated the interface reaction and crystallography of the electroless plated copper film (~0.2 μm thick) catalyzed by plasma immersion ion implanted (PIII) Pd on the 150-Å-thick amorphous tantalum nitride (*a*-Ta:N) barrier layer. The copper plated specimens were annealed at various temperatures in an ambient atmosphere of 90% nitrogen + 10% hydrogen mixed gases. Sheet resistivity, Auger electron spectroscopy (AES) analyses showed that the PIII Pd atoms were diffused into the copper layer from the interface of *a*-Ta:N and copper layers after 500 °C annealing for 1 h. Results based on x-ray diffraction (XRD) and high-resolution transmission electron microscopy (HRTEM) showed a phase transformation from *a*-Ta:N into crystallized Ta_2N phase at annealing. The Cu(111) texture was strengthened at 300 °C annealing for 1 h because of the relaxation of the residual stress and recovery of the copper film. The texture was reduced at the 500 °C annealing for 1 h because of the copper grain growth. The adhesion strength of copper films on *a*-Ta:N barrier layer was enhanced by the annealing because of the interdiffusion of copper layer, Pd clusters and *a*-Ta:N barrier layer. The annealing temperatures lower than 300 °C help to reduce the electric resistivity of copper film, to strengthen the Cu(111) preferred orientation, and to enhance the adhesion strength of copper films on *a*-Ta:N layer. However, the specimen annealed at 500 °C manifested the diffusion of Pd atoms into the copper film and resulted in a significant increase of the electric resistivity of copper film. [DOI: 10.1116/1.1465448]

I. INTRODUCTION

Copper is an attractive material for interconnection due to its lower electrical resistivity and better electromigration resistance than aluminum and Al-based alloys.[1,2] Self-annealing at room temperature is a well-known phenomenon for purely as-deposited copper films. This property leads to changes in the electrical, mechanical, and microstructural characteristics of the copper films.[3–5] In order to reduce the internal stress energy, the dislocation tends to segregate around the grains or to form low- angle grain boundaries to recover the mechanical properties to the copper films' equilibrium state. This so-called self-annealing has been observed to take place over a period of hours, or even weeks, which tends to stabilize the copper film.[3,6] Therefore, a post-annealing treatment is usually necessary for the stabilization of the as-deposited copper film's character in the short term to make copper in trenches/vias producing a reflowed (copper atoms surface diffusion) situation to achieve the goal which repairs the defects of interconnections.[7,8]

Electroless copper plating is a promising and efficient method to deposit the highly selective and conformal copper for filling high-aspect ratio trenches and vias, especially as the trenches/vias further scale down. For example, if they are smaller than 0.1 μm, the fabrication of a seed layer for copper electroplating will be difficult. In such a case, electroless copper plating will become progressively more important. Besides, electroless copper plating also benefits from its low tool cost and low temperature process.

[a)]Author to whom correspondence should be addressed; electronic mail: hcshih@mse.nthu.edu.tw

Customarily, a metal seed layer such as Cu, Pd, Au, Ni, Ag or Pt, etc.,[9] is necessary to activate electroless Cu plating. Recent work has established large area plasma immersion ion implantation (PIII)[10–12] or metal vapor vacuum arc[13] as Pd-seeding techniques for copper electroless plating on silicon wafer. The gradual transition from a Pd-rich to a Pd-deficient surface is also expected to improve the adhesion of the plated Cu film.[14]

The objective of this study was to combine the process of PIII and electroless plating techniques in the formation of a copper film on the as-deposited wafers consisting of *a*-Ta:N and fluorosilicate glass (FSG) layers which were consecutively deposited on Si, and to analyze the Cu/*a*-TaN interfacial and crystallographic structures after the specimen being annealed.

II. EXPERIMENT

A. Coating preparation

The substrates used in all experiments were 8-in. *p*-type (100) silicon wafers on which a 1.2-μm-thick chemical vapor deposition FSG film was grown as an interlayer of the low-*k* dielectric layer. Ionized metal plasma was used to deposit *a*-Ta:N layer ($\sim$ 15 nm) on the FSG layer as an adhesion and diffusion barrier layer. Figure 1 shows the process of electroless Cu deposited on the Pd clusters which were sputtered from a negatively biased target (Pd) and ionized in an argon inductively coupled plasma. The Pd ions were adequately implanted into the substrate with a dc pulsed negative bias voltage ($\sim$4 kV; 13.56 MHz), and the implanted Pd doses were controlled at 5×10^{14} cm^{-2}. The PIII Pd treated specimens were then put into the electroless Cu plating bath for Cu plating, whose chemical composition is shown in Table I. The bath temperature was kept in the range of 50–65 °C, with a solution *p*H of 11–13.

B. Electroless copper plating

The chemistry of the electroless plated Cu used in this study was the redox reactions between Cu-EDTA complex ions and formaldehyde.[9] The plating bath was alkalined with tetramethyl ammonium hydroxide (TMAH) to control the bath *p*H. The stabilizer 2, 2′-bipyridine could trap Cu^+ ions to prevent Cu deposition in the plating solution spontaneously.[15] Polyethyleneglycol was added as a surfactant to reduce the surface tension, thereby inhibiting the formation of hydrogen gas bubbles on the plating of Cu. The thickness of electroless plated copper films on wafers was about 0.2 μm. The interface of copper and *a*-Ta:N, owing to the Pd clusters in the interface,[13] does not form a continuous layer. Therefore, in this article, the assembly of Cu/(Pd)/*a*-Ta:N will be designated to represent the interfacial structure between electroless plated copper and *a*-Ta:N layer.

C. Annealing

The electroless plated copper specimens were annealed in a tube furnace with an atmosphere of 90% nitrogen and 10% hydrogen mixed gases for preventing the surface oxidation of the specimen being annealed at 150, 300, and 500 °C for 1 h. The oxygen partial pressures (P_{O_2}) of the mixed gases during the annealing process were monitored by an oxygen sensor[16–19] (15 mol% CaO-doped ziconia). The detected P_{O_2} and the equilibrium[20] P_{O_2} in various annealing temperatures are listed in Table II.

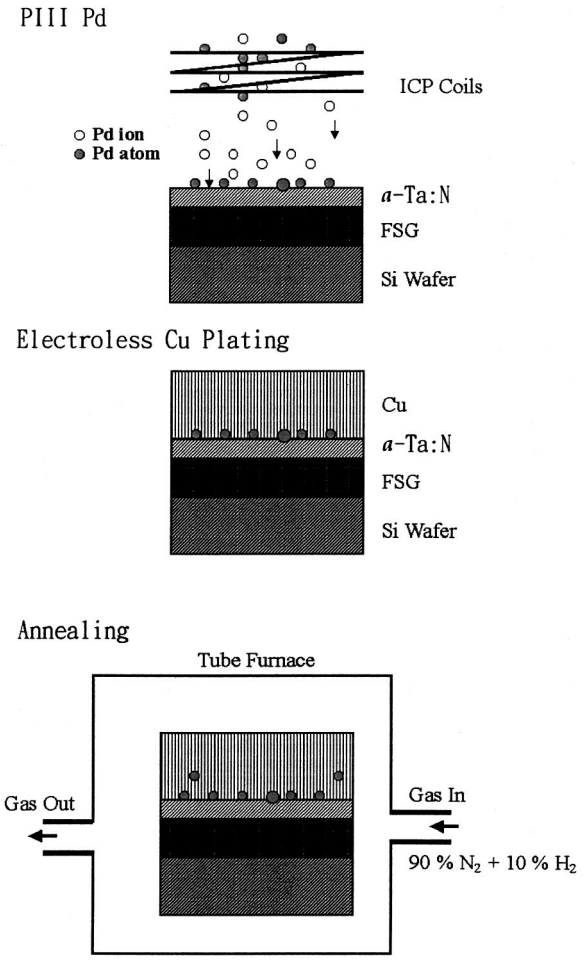

FIG. 1. Process sequences for the formation of Cu electroless plating on a nonpatterned wafer *a*-Ta:N/FSG.

F. Characterization

The microstructure was analyzed using JEOL JEM-4000EX HRTEM and crystallographic phases were determined using MAC Sci. MXP-18 XRD with Cu$K\alpha$ radiation. The sheet electric resistivity was measured with a four-point

TABLE I. Chemical composition of the electroless Cu plating solution employed in this study.

Solution containing	Range (g/L)
$CuSO_4\cdot5H_2O$	6–10
EDTA	25–35
TMAH	100–140
PEG (polythyleneglycol)	0.5–1.5
2, 2′-bipyridine	0.1–1.2
HCHO (37%)	6–10

TABLE II. The detected and equilibrium (see Ref. 20) oxygen partial pressure (P_{O_2}) in the annealing furnace.

Annealing temperature (°C)	Detected P_{O_2} (atm)	Theorem equilibrium P_{O_2}(atm)		
		CuO[a]	Cu_2O[b]	Ta_2O_5[c]
150	$2.5\times10-7$	1.8×10^{-29}	7.4×10^{-35}	4.2×10^{-92}
300	8.5×10^{-25}	1.3×10^{-19}	5.6×10^{-24}	6.5×10^{-66}
500	3.5×10^{-30}	2.0×10^{-12}	4.9×10^{-16}	8.3×10^{-47}

[a] $Cu+1/2O_2=CuO$, $\Delta G^0=-152522+85.253T$.
[b] $2Cu+1/2O_2=Cu_2O$, $\Delta G^0=-168406+71.254T$.
[c] $2Ta+21/2O_2=Ta_2O_5$, $\Delta G^0=-2025056+412.542T$.

probe and the average grain size of copper was determined by the linear intersection method.[21] The depth of the interdiffusion of the Cu/(Pd)/*a*-Ta:N assembly was analyzed by PHI 670 AES depth profile techniques.

The adhesion strength was evaluated by the pull-up test, and the peeled area was characterized by PHI 1600 x-ray photoelectron spectroscopy (XPS) with Al $K\alpha$ radiation with a probe size of 0.8 mm diameter. The pull test measurements were carried out using a Romulus III Universal Tester with a aluminum stud face diameter of 3 mm, and the pull speed was 5 mm/min. Samples with epoxy coated studs were fixed on epoxy coated backing plates and were cured at 150 °C for 1.5 h in nitrogen ambient atmosphere. At least four samples were used to determine the average breaking point.

III. RESULTS AND DISCUSSION

A. Electric resistivity

1. PIII Pd catalyst

Figure 2 shows the sheet electric resistivity and grain size variation of the electroless plated copper specimens with respect to the annealing temperature. Figure 2(a) indicates that if the electroless plated copper films were catalyzed by PIII Pd, the electric resistivity of the annealed copper film drastically decreases with increasing temperature to a lowest value of 2.29 $\mu\Omega$ cm at 300 °C, because annealing can promote the recovery, recrystallization and grain growth of the as-deposited copper film.[3,6] Consequently, the crystalline defect reduction is the main reason for the observed decrease of the electric resistivity. However, as the temperature further increases to 500 °C, there is a slight increase of the sheet resistivity to 2.51 $\mu\Omega$ cm.[22]

The recrystallized copper plate is significantly influenced by the degree of cold work. If the cold-worked strain ratio is not high enough, such as <3% for copper alloy,[19] recrystallization will not occur even though annealed at higher temperature for a longer time. The recovery and recrystallization of the deposited copper film can take place at room temperature simultaneously, due to its submicron thickness and residual high density dislocation in the copper film.[23]

Figure 2(a) shows that the copper grain annealed at 150 °C does not grow substantially, but on the contrary, the resistivity of copper film decreases drastically, accounting for the recovery of the copper film. For the specimen annealed at 300 °C, there is only a slight increase in grain size (~132 nm) and a major increase (~350 nm) at 400 °C. This indicates that the copper film has been partially recrystallized at 300 °C and is heading for the grain growth as temperature increases to 400 °C. In addition, copper grain size is increased up to ~694 nm by annealing at 500 °C. Larger copper grains have less grain boundaries and therefore decrease the resistivity of the copper film. However, it is interesting to note that there is not clearly deference of the resistivity after 300 °C, which reaches a value of 2.32 $\mu\Omega$ cm at 400 °C. After 500 °C annealing, the electric resistivity is significantly increased to 2.51$\mu\Omega$ cm. The use of Pd as catalyst is the most often used method to activate the surface for the subsequent electroless copper plating. Nevertheless, the resistivity of Pd (10.54 $\mu\Omega$ cm) is about six times higher than that of Cu (1.67 $\mu\Omega$ cm).[24] Under the circumstances, $PdCu_6$ intermetallic compound[25] is the most plausible phase at 400 °C. Henceforth, Fig. 2(a) implies that higher temperatures (>300 °C) significantly increase the resistivity which may have resulted from the diffusion of Pd atoms into the copper film.

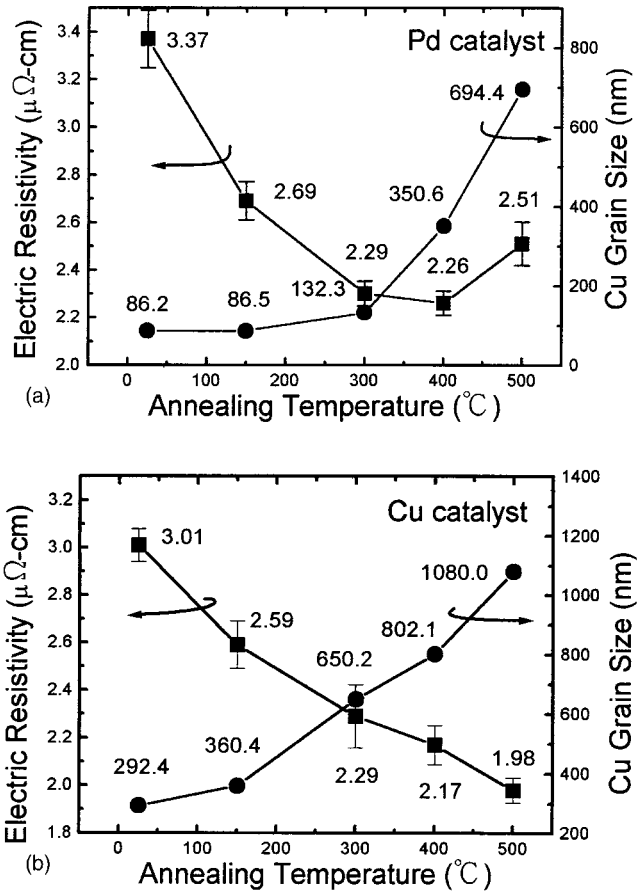

FIG. 2. Sheet resistivity and grain size vs annealing temperature of the electroless plated Cu catalyzed by PIII (a) Pd and (b) Cu seeds.

2. PIII Cu catalyst

Through the utilization of the self-catalytic effect, PIII Cu as seeds applied on *a*-Ta:N was also explored in this study in order to gain an insight as well as a comparison with PIII Pd

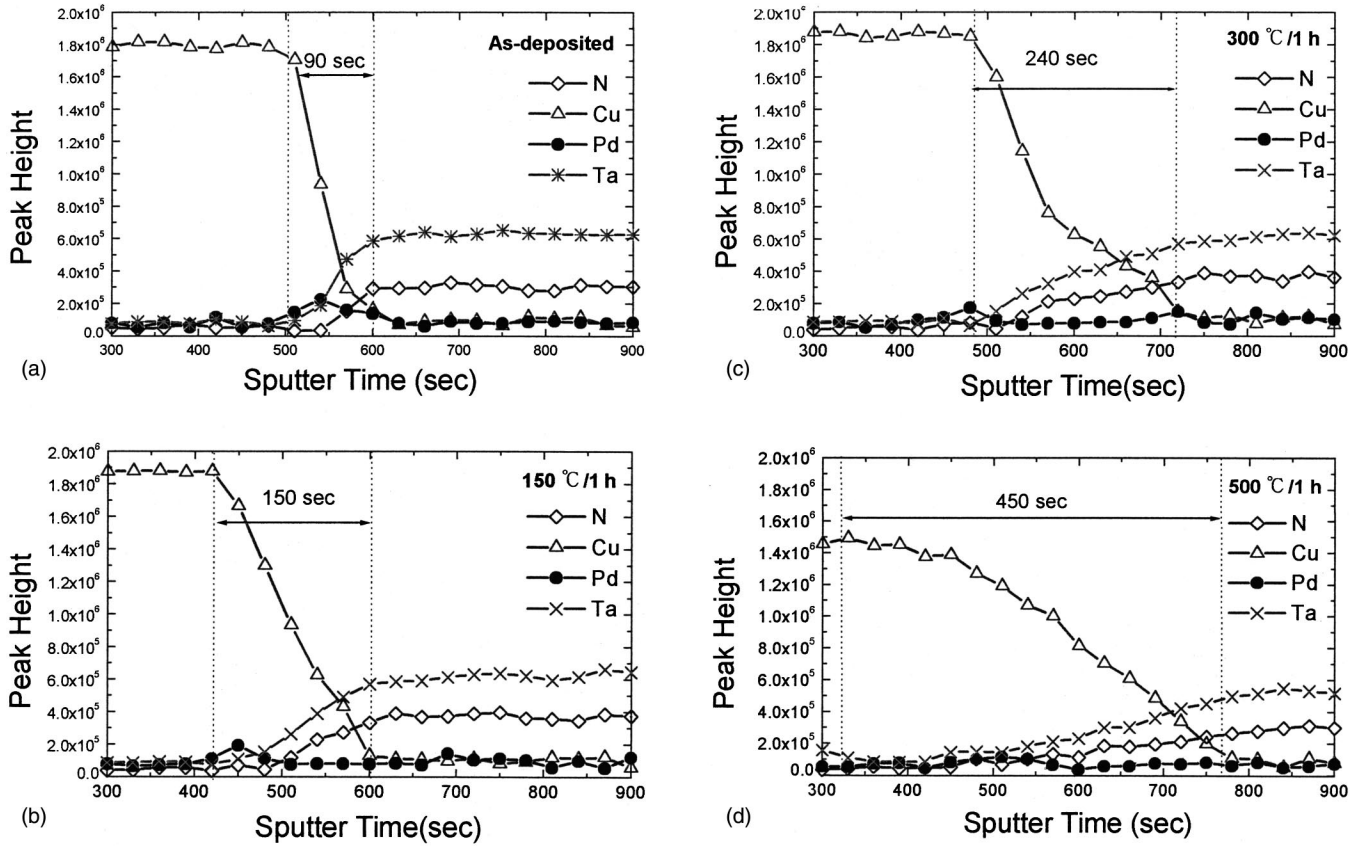

FIG. 3. AES depth profile analyzing Cu/(Pd)/*a*-TaN interface with (a) annealing free and annealed at (b) 150 °C, (c) 300 °C, and (d) 500 °C.

as catalyst to the formation of the electroless Cu plate. The sheet resistivity and grain size of the electroless plated copper films as a function of the annealing temperature are shown in Fig. 2(b). The electric resistivity of the as-deposited copper film is 3.01 $\mu\Omega$ cm, and is decreased with increasing annealing temperature. Unlike PIII Pd seeds, the resistivity for PIII Cu seeds drops monotonically to 1.98 $\mu\Omega$ cm at 500 °C. This proves that Pd as seeds for electroless copper plating will invariably encounter the problem of high electric resistivity in the future ultralarge scale integration copper interconnect metallization process.

B. Interface of the Cu/(Pd)/*a*-Ta:N assembly

As shown in Fig. 3, the AES depth profiles are measured in order to obtain more information on the Cu/(Pd)/*a*-Ta:N interfacial reaction(s). Figure 3(a) is the AES spectra of the as-deposited specimen without subsequent annealing, thus the Cu/(Pd)/*a*-Ta:N interface is easily discernible. The interface is significantly broadened at 150 and 300 °C, as shown in Figs. 3(b) and 3(c). The content of Pd atoms maintains a stable level in the interface; no abrupt diffusion signals are observed. These spectra indicate that these layers can exist up to 300 °C without evidence of severe intermixing. As the temperature increases to 500 °C, the interdiffusion among Cu, Pd and Ta are even more significant, as shown in Fig. 3(d). The result of AES depth profile indicates that as the annealing temperature increases, the interdiffusion zone of the Cu/(Pd)/*a*-Ta:N interface tends to be widened, as shown in Fig. 4.

As for the diffusion of Ta into the copper film in the process of annealing, two reactive mechanisms have been proposed:[26] (1) If there is enough oxygen present in the annealing furnace, the diffusion of Ta may occur since Ta has a

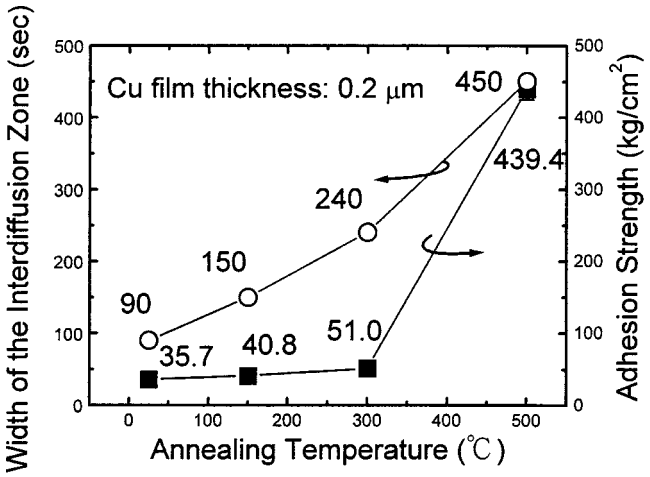

FIG. 4. Relation between adhesion strength and the width of the interdiffusion zone of the electroless plated copper film on the nonpatterned wafer enhanced by increasing the annealing temperature.

higher affinity towards oxygen, and (2) It is also possible that stresses incorporated into the Ta-based layer during the deposition enhance the diffusion of Ta. In this research, the oxygen partial pressures (P_{O_2}) are high enough to form a stable phase of Ta_2O_5, as shown in Table II. The *a*-Ta:N layer also accumulates residual stress in the PIII Pd process. Therefore, the two reactive mechanisms of the Ta diffusion are co- operated in the Cu/(Pd)/*a*-Ta:N assembly.

C. Adhesion strength

The adhesion strength of the electroless plated copper film on the Cu/(Pd)/*a*-Ta:N assembly as a function of the annealing temperature is shown in Fig. 4. The adhesion strength of the as-deposited copper film without annealing is 35.7 kg/cm^2; significant increase occurs at >300 °C and reaches 439.4 kg/cm^2 at 500 °C. The annealing process will promote the interdiffusion crossing the interfaces and relax the residual stress[27] of the Cu/(Pd)/*a*-Ta:N assembly, which are the two major reasons for the increased adhesion strength as a result of the annealing treatment. Figure 4 also implies that adhesion strength of the Cu film is strongly dependent on the width of the interdiffusion of the Cu/(Pd)/*a*-Ta:N.

Figure 5(a) shows the OM image of a continuous and smooth morphology of the peeled area of the specimen without previous annealing. Figure 5(b) shows the XPS survey spectra of the un-peeled area, where only Cu and O optical electron peaks are observed. However, the peeled area possesses strong Ta and Cu optical electron peaks in the survey spectrum and weak Pd 3*d* peaks in the fine scan spectrum; no clear Si peaks in the survey spectrum were detected, as shown in Fig. 5(c), indicating that the split plane for separation is located in between the copper and *a*-Ta:N interface of the Cu/(Pd)/*a*-Ta:N assembly.

As shown in Fig. 6(a), the OM image of the specimen annealed at 300 °C exhibits a discontinuous surface morphology of the peeled plane. By characterizing the area A using XPS as shown in Fig. 6(b), the Si optical electron peaks are clearly observed, but no significant signals from Cu, Pd and Ta are detected. However, the result from the area B, as shown in Fig. 6(c), is essentially the same as Fig. 5(c). The XPS measurements indicate that the separation after peeling covers the interfaces of *a*-Ta:N/FSG (area A) and Cu/*a*-Ta:N (area B). Annealing treatment helps to enhance the adhesion strength of the copper film to the *a*-Ta:N layer. Similar results were observed on the other stripped half. Therefore, it may be concluded that the adhesion strength is higher than the cohesion strength of the Cu/(Pd)/*a*-Ta:N assembly.

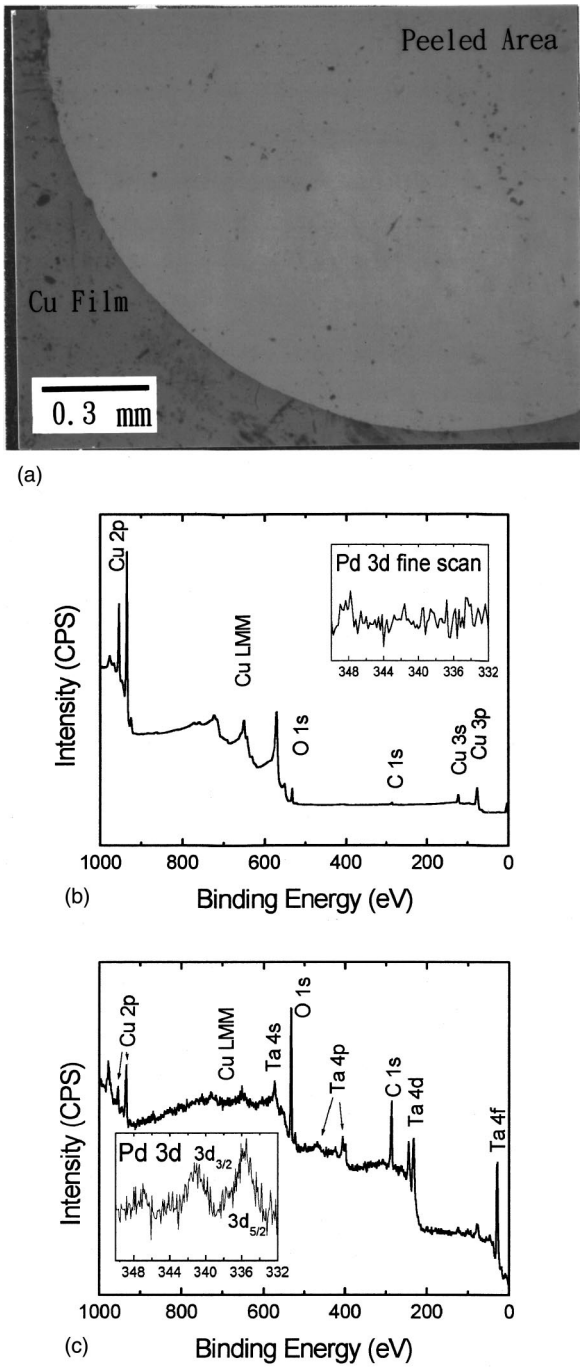

FIG. 5. Pull-up adhesion strength test of the annealing-free specimen: (a) OM image, (b) XPS spectra of the unpeeled area, and (c) XPS spectra of the peeled area.

D. Crystallography of the copper films and barrier layers

Figure 7(a) shows the XRD patterns obtained for the specimens of the Cu/(Pd)/*a*-Ta:N assembly without annealing and annealed at 150, 300, and 500 °C. From the normalized peak heights, it was found that the copper film as deposited mainly manifests Cu(111) preferred orientation. The peak height ratio of Cu(111)/Cu(200) as given by in the Joint Committee on Powder Diffraction Standards (JCPDS)[28] card is near 2.17. As shown in Fig. 7(b), the peak height ratio value of Cu(111)/Cu(200) increases at the annealing temperature $\leqslant$ 300 °C. At 300 °C, the ratio of Cu(111)/Cu(200) reaches a maximum of 28.35, indicating that the copper film is highly ⟨111⟩ textured. It is well known that the copper film with a strong ⟨111⟩ texture can enhance its electromigration resistivity performance, because of the reduced degree of anisotropy in grain-boundary transport.[29] Hence, the strong Cu(111) preferred orientation of the specimen annealed at 300 °C is significant in this research.

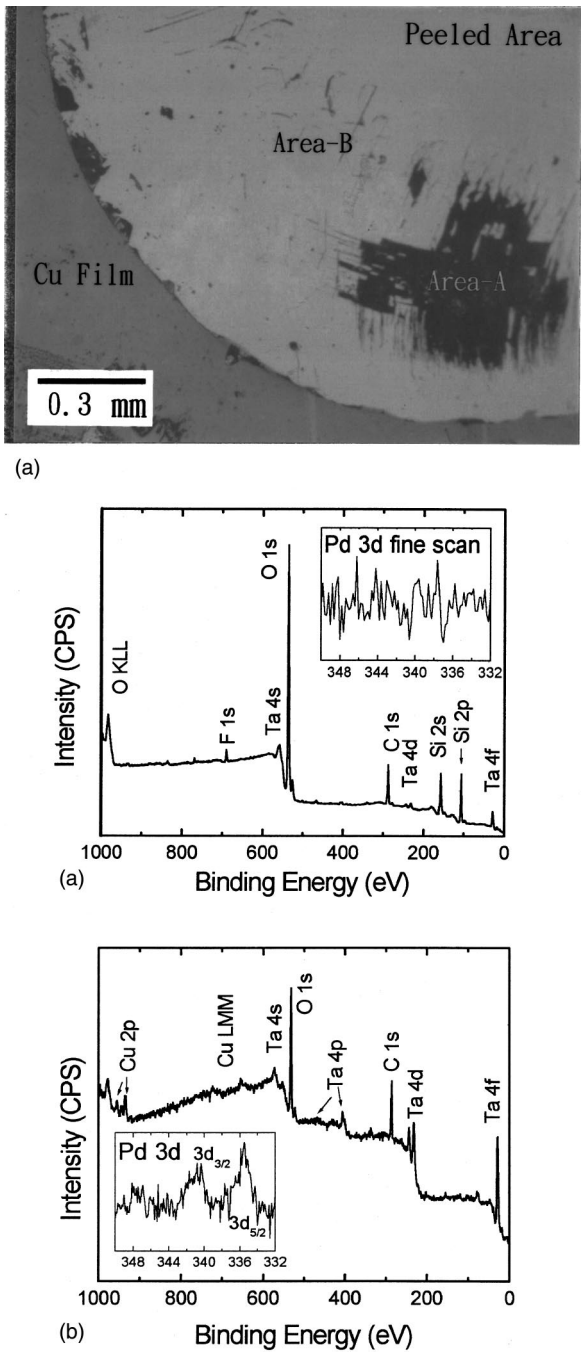

FIG. 6. Pull-up adhesion strength test after the specimen annealed at 300 °C: (a) OM image and (b) XPS spectra of the area A, and (c) XPS spectra of the area B on the peeled area.

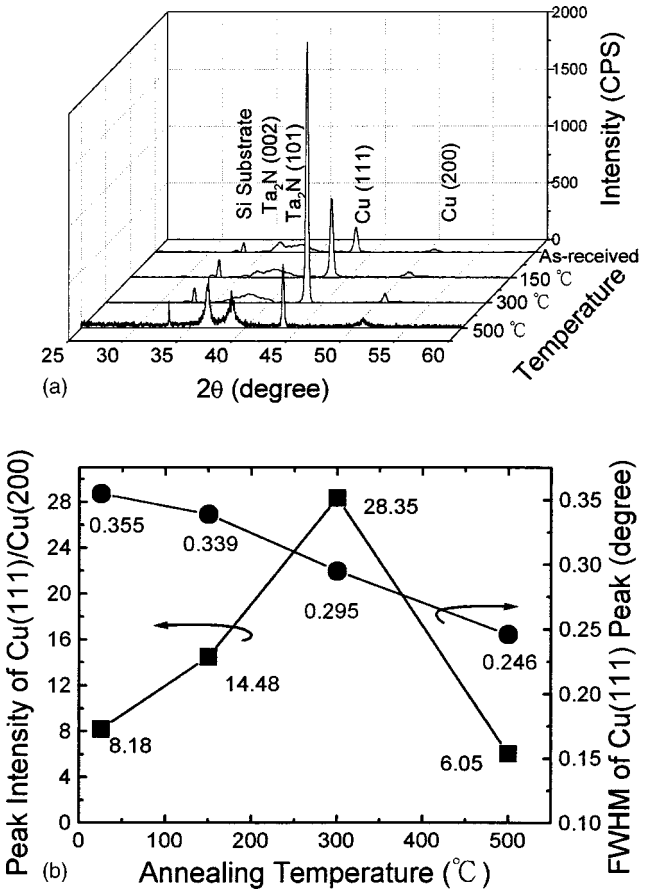

FIG. 7. Electroless plated copper films on *a*-TaN/FSG wafers with various annealing temperatures: (a) XRD patterns and (b) the Cu(111)/Cu(200) normalized peak height ratio and FWHM of Cu(111) peak as a function of temperature.

Recent studies[30,31] have shown that plating and processing conditions have a strong influence on the initial as well as the preferred orientation texture of electroless plated copper film. The crystallographic orientations of the diffusion barrier and seed layer have also been shown to influence the texture of plated copper film.[31–33]

While the peak ratio of Cu(111)/Cu(200) is increased with the increasing annealing temperature up to 300 °C, the full width of half maximum (FWHM) of the Cu(111) peak is simultaneously decreased consistently with the annealing temperature up to 500 °C. These results indicate that the recrystallization as well as the defects recovery[34] of the residual stress relaxation of the electroless plated copper films enhance the (111) texture in the annealing process. Since Cu(111) is the most close-packed plane and is the preferred orientation in this study, it may be concluded that the system free energy of the Cu/(Pd)/*a*-Ta:N assembly tends to minimize through the predominance of the (111) plane which has a lower surface free energy than the (200) plane.[35] Hence, the peak ratio of Cu(111)/Cu(200) is particularly noticeable at 300 °C in the annealing process driven by the residual stress relaxation in order to reduce the surface free energy of the copper film.

The XRD patterns [Fig. 7(a)] also show the strong Ta_2N(002) and Ta_2N(101) peaks for the specimen annealed at 500 °C. The maximum of the Cu(111)/Cu(200) peak ratio is 28.35 for the specimen annealed at 300 °C, but the peak ratio decreases to 6.05 as temperature further increases to 500 °C, indicating that the strong Cu(111) texture has been reduced at >300 °C. On the other hand, the pronounced increase of the copper grain sizes [Fig. 2(a)] indicates that the copper film has been recrystallized and a significant grain growth would turn the textured copper grains into randomly orientated grains. Figure 2(a) also shows that there is no

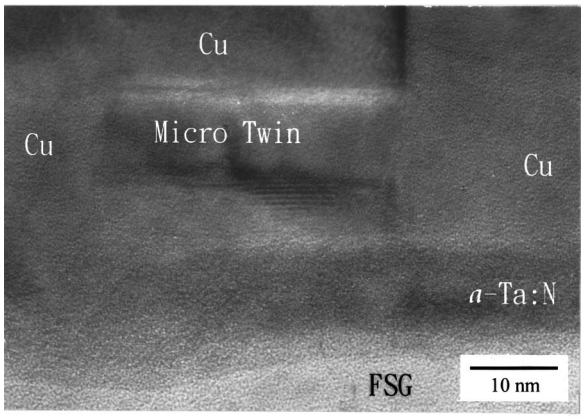

(a)

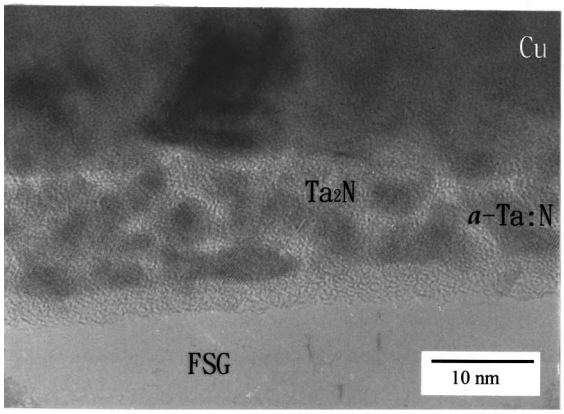

(b)

FIG. 8. Cross-sectional HRTEM images of the Cu/(Pd)/*a*-TaN/ FSG interfaces: (a) annealing free and (b) annealed at 300 °C.

measureable difference of copper grain size at temperature <300 °C. However, Fig. 7(b) shows that FWHMs are of significant difference in the temperature range, which seems to contradict the grain size measurement at <300 °C. In fact, it is due to the quantity of FWHM combined effect from microstress and grain size in the film. The FWHM changes at <300 °C are primarily to the relaxation from the microstress, not from the grain growth.

Figure 8(a) shows the cross-sectional HRTEM image obtained from the Cu/(Pd)/*a*-Ta:N assembly without annealing. The HRTEM image shows that the grain boundaries of the electroless plated copper film are vertical to the *a*-Ta:N layer; microtwins and stacking faults are the major crystalline defects, whose grain boundaries are parallel to the Cu/*a*-Ta:N interface. Hence, the as-deposited copper film provides a strong ⟨111⟩ texture of the columnar copper grains. The Cu(111) preferred orientation is also strengthened by the relaxation of the residual stress for the Cu/(Pd)/*a*-Ta:N assembly annealed at 300 °C.

For the specimen annealed at 300 °C, the cross-sectional HRTEM image shows the occurrence of nano-crystallites which can be unambiguously resolved in the *a*-Ta:N layer. The corresponding crystallographic structure can be distinguished by the reciprocal lattice image from the real lattice space. We have found that the hexagonal Ta_2N nanocrystallites (~3 nm) have been formed in *a*-Ta:N matrix. Because the doses of palladium is very low, the peak formed by metallic Pd or Pd compounds is not observed in the XRD patterns; no clearly crystallized Pd is ever found in the interface of copper film and barrier layer (Cu/*a*-TaN), as shown in Figs. 8(a) and 8(b). However, the XRD patterns also indicate that the hexagonal Ta_2N has been precipitated in the matrix of *a*-Ta:N with long range ordered crystals of the 500 °C annealed specimen. However, also known from the HRTEM image, there exists short range ordered Ta_2N nanocrystallites formed in the *a*-Ta:N matrix in the annealing process of at least at 300 °C.

IV. Conclusions

(1) As the annealing temperature increases, the interdiffusion zone of the Cu/(Pd)/*a*-Ta:N assembly tends to be widened; the interdiffusion zone increases with increasing annealing temperatures.

(2) When PIII Pd is used as a catalyst, the electric resistivity of annealed copper films decreases with increasing annealing temperature, e.g., to 2.29 $\mu\Omega$ cm at 300 °C, but slightly increases to 2.51 $\mu\Omega$ cm at 500 °C, resulting from the diffusion of the Pd atoms into the copper film. When PIII Cu is used as self-catalyst, the electric resistivity for the as-deposited copper film (3.01$\mu\Omega$ cm), decreases with increasing annealing temperature to 1.98 $\mu\Omega$ cm at 500 °C.

(3) The adhesion strength of the nonannealed copper film on barrier layer *a*-Ta:N is 35.7 kg/cm^2 and increases to 439.4 kg/cm^2 at 500 °C; the adhesion strength is strongly dependent on the width of the interdiffusion zone of the Cu/(Pd)/*a*-Ta:N assembly.

(4) The annealing-free copper film provides a strong ⟨111⟩ texture, made of columnar grains whose grain boundaries are vertical with the *a*-Ta:N layer. The XRD peak ratio of Cu(111)/Cu(200) increases to 28.35 at 300 °C and decreases to 6.05 at 500 °C, indicating that the strong Cu(111) texture has been reduced at 300 °C.

ACKNOWLEDGMENTS

The authors would like to acknowledge the financial support for this research from the National Science Council of the Republic of China, under NSC No. 90-2218-E-007-003. The authors would also like to acknowledge Professor F.-H. Lu of the Department of Materials Engineering, National Chung Hsing University, for his annealing furnace with oxygen sensors; without his facilities, this research would not be possible.

Presented at the IUVSTA 15th International Vacuum Congress and the AVS 48th International Symposium and the 11th International Conference on Solid Surfaces, San Francisco, California, 28 October–2 November 2001.

[1]C. W. Park and R. W. Vook, Thin Solid Films **226**, 328 (1993).
[2]D. Gupta and P. S. Ho, Thin Solid Films **72**, 339 (1980).
[3]C. Link and M. E. Gross, J. Appl. Phys. **84**, 5547 (1998).
[4]S. H. Brongersma, E. Richard, I. Vervoort, H. Bender, W. Vandervorst, S. Lagrange, G. Beyer, and K. Maex, J. Appl. Phys. **86**, 3642 (1999).
[5]J. M. E. Harper, C. Cabral, Jr., P. C. Andricacos, L. Gignac, I. C. Noyan, K. P. Rodbell, and C. K. Hu, J. Appl. Phys. **86**, 2516 (1999).
[6]S. P. Hau-Riege and C. V. Thompson, Appl. Phys. Lett. **76**, 309 (2000).

[7]S. Y. Lee, D. W. Kim, S. K. Rha, C. O. Park, and H. H. Park, J. Vac. Sci. Technol. B **16**, 2902 (1998).
[8]L. J. Friendrich, S. K. Dew, M. J. Brett, and T. Smy, J. Vac. Sci. Technol. B **17**, 186 (1999).
[9]Y. Shacham-Diamand, V. M. Dubin, and M. Angyal, Thin Solid Films **262**, 93 (1995).
[10]X. Y. Qian, D. Carl, J. Benasso, N. W. Cheung, M. A. Lieberman, J. E. Galvin, R. A. MacGill, and M. I. Current, Nucl. Instrum. Methods Phys. Res. B **55**, 888 (1991).
[11]X. Y. Qian, M. H. Kiang, J. Huang, D. Carl, N. W. Cheung, M. A. Lieberman, I. G. Brown, K. M. Yu, and M. I. Current, Nucl. Instrum. Methods Phys. Res. B **55**, 884 (1991).
[12]J. H. Lin, Y. Y. Tsai, S. Y. Chiu, T. L. Lee, C. M. Tsai, P. H. Chen, C. C. Lin, M. S. Feng, C. S. Kou, and H. C. Shih, Thin Solid Films **377-378**, 592 (2000).
[13]G. K. Muralidhar, S. Bhansali, A. Pogany, and D. K. Sood, J. Appl. Phys. **83**, 5709 (1998).
[14]M. H. Kiang, M. A. Lieberman, N. W. Cheung, and X. Y. Qian, Appl. Phys. Lett. **60**, 2767 (1992).
[15]K. Kondo, K. Kojima, N. Ishida, and M. Irie, J. Electrochem. Soc. **140**, 1598 (1993).
[16]F.-H. Lu, and H.-Y. Chen, Thin Solid Films **355-356**, 374 (1999).
[17]J. W. Patterson, E. C. Borgen, and R. A. Rapp, J. Electrochem. Soc. **114**, 752 (1967).
[18]A. J. Moulson and J. M. Herbert, *Electroceramics: Materials, Properties, Applications* (Chapman and Hall, Cambridge, 1990), pp. 150–160.
[19]I. Riess, H. Janczikowski, and J. Nölting, J. Appl. Phys. **61**, 4931 (1987).
[20]Y. K. Rao, *Stoichiometry and Thermodynamics of Metallurgical Process* (Cambridge University Press, Cambrige, 1985), pp. 883, 884.
[21]ASTM Standards No. E 112-85.
[22]R. E. Reed-Hill and R. Abbaschian, *Physical Metallurgical Principles*, 3rd ed. (PWS, Boston, 1994), pp. 247, 248.
[23]D. S. Stoychev, I. V. Tomov, and I. B. Vitanova, J. Appl. Electrochem. **15**, 879 (1985).
[24]*CRC Handbook of Chemistry and Physics* 75th edited by D. R. Line and H. P. R. Frederikse (CRC, Boca Raton, 1994), pp. 12-40 and 12-41.
[25]D. Y. Shih, C. A. Chang, J. Paraszczak, S. Nunes, and J. Cataldo, J. Appl. Phys. **70**, 3052 (1991).
[26]T. Laurida, K. Zeng, J. K. Kivilahti, J. Molarius, and I. Suni, J. Appl. Phys. **88**, 3377 (2000).
[27]C. H. Seah, S. Mridha, and L. H. Chan, J. Vac. Sci. Technol. A **17**, 1963 (1999).
[28]JCPDS Card No. 04-0836.
[29]D. B. Knorr and K. P. Rodbell, J. Appl. Phys. **79**, 2409 (1996).
[30]S. P. Kim, H. M. Choi, and S. K. Choi, Thin Solid Films **322**, 298 (1998).
[31]H.-H. Hsu, K.-H. Lin, S.-J. Lin, and J.-W. Yeh, J. Electrochem. Soc. **148**, C47 (2001).
[32]K. Abe, Y. Harada, and H. Onoda, Appl. Phys. Lett. **71**, 2782 (1997).
[33]J. Li and Y. Shacham-Diamand, J. Electrochem. Soc. **39**, L37 (1992).
[34]G. K. Williamson and W. H. Hall, Acta Metall. **1**, 22 (1953).
[35]D. A. Porter and K. E. Easterling, *Phase Transformations in Metals and Alloys* (Chapman and Hall, London, 1992), p. 112.